Sains Malaysiana 53(5)(2024): 1133-1147
*http://doi.org/10.17576/jsm-2024-5305-13*

# Efficient Removal of Pb(II) Ion using $TiO_2$/ZnO/$SiO_2$ Nanocomposite from Aqueous Solutions *via* Adsorption-Photocatalysis Process

(Penyingkiran Cekap Ion Pb(II) menggunakan Nanokomposit $TiO_2$/ZnO/$SiO_2$ daripada Larutan Akua melalui Proses Penjerapan-Fotokatalisis)

Dadan Hadian[1,2], Anita Alni[3], Aep Patah[4], Nurrahmi Handayani[1,5] & Muhammad Ali Zulfikar[1,*]

[1]*Analytical Chemistry Research Group, Institut Teknologi Bandung, Indonesia*
[2]*Center for Ceramics, Ministry of the Industry Republic of Indonesia, Indonesia*
[3]*Organic Chemistry Research Group, Institut Teknologi Bandung, Indonesia*
[4]*Inorganic and Physical Research Group, Institut Teknologi Bandung, Indonesia*

[5]*Research Center for Nanosciences and Nanotechnology, Institut Teknologi Bandung, Indonesia*

*Received: 14 November 2023/Accepted: 20 March 2024*

ABSTRACT

This research aims to investigate the usage of a $TiO_2$/ZnO/$SiO_2$ (TZS) composite prepared via a 24-h hydrothermal process at 180° C to remove Pb(II) through adsorption-photocatalysis. Pb(II) exposure has known health risks, making this study significant. The research explores the impact of pH, the nanocomposite quantity, and contact time in the process. Adsorption-photocatalysis was carried out in the dark for 60 min, followed by irradiation with a 160-watt mercury lamp. The adsorption process of Pb(II) ion removal adhered to the pseudo-second-order model regarding kinetics, while the adsorption isotherm corresponded to the Freundlich isotherm. Additionally, the assessment of photocatalysis kinetics showed that the removal of Pb(II) ions followed a pseudo-first-order model, resulting in a 99.58% elimination of Pb(II) ions. Post-adsorption-photocatalytic treatment, a yellowish precipitate was observed. The XRD pattern result of the yellowish precipitate confirmed the presence of PbO as the formed Pb phase. The study concludes that the $TiO_2$/ZnO/$SiO_2$ nanocomposite as adsorbent-photocatalyst is a highly effective, efficient, and promising method to remove Pb(II) contamination from aqueous solutions.

Keywords: Adsorption-photocatalytic; removal Pb(II) ion; $TiO_2$/ZnO/$SiO_2$ composite

ABSTRAK

Penyelidikan ini bertujuan untuk mengkaji penggunaan nanokomposit $TiO_2$/ZnO/$SiO_2$ (TZS) yang disediakan melalui proses hidrotermal selama 24 jam pada suhu 180 °C untuk menyingkirkan Pb(II) melalui penjerapan-fotokatalisis. Pendedahan Pb(II) diketahui membawa risiko kesihatan, menjadikan kajian ini penting. Penyelidikan ini meneroka impak pH, kuantiti nanokomposit dan masa sentuhan dalam proses tersebut. Penjerapan-fotokatalisis dilakukan dalam gelap selama 60 minit, diikuti oleh penyinaran dengan lampu merkuri 160 watt. Proses penjerapan pengeluaran ion Pb(II) menurut model kinetik pseudo-tertib kedua, manakala isoterma penjerapan sejajar dengan isoterma Freundlich. Tambahan pula, penilaian kinetik fotokatalisis menunjukkan bahawa penyingkiran ion Pb(II) mengikuti model pseudo-tertib pertama, menghasilkan penghapusan ion Pb(II) sebanyak 99.58%. Selepas rawatan penjerapan-fotokatalisis, endapan kuning diperhatikan. Hasil corak XRD bagi endapan kekuningan mengesahkan kehadiran PbO sebagai fasa Pb yang terbentuk. Kajian ini menyimpulkan bahawa penjerap-fotokatalis nanokomposit $TiO_2$/ZnO/$SiO_2$ adalah kaedah yang sangat berkesan, cekap dan berpotensi untuk menyingkirkan pencemaran Pb(II) daripada larutan akua.

Kata kunci: Komposit $TiO_2$/ZnO/$SiO_2$; penjerapan-fotokatalitik; penyingkiran ion Pb(II)

## Introduction

Lead, a dangerous heavy metal, is commonly found as a pollutant in wastewater derived from multiple origins, including galvanizing industries, urban sewage systems, mines, battery manufacturing, paper mills, alloy production, ceramic and glass industries, as well as pigment manufacturing (Wahyuni et al. 2022; Yang & Zhang 2010; Zhang et al. 2020). Exceeding prescribed tolerance levels of these hazardous metals can lead to a host of health issues, such as neurological, respiratory, urinary, and cardiovascular disorders, cancer, aggressive behavior, high blood pressure, sleep problems, and lightheadedness (Balali-Mood et al. 2021). When Pb(II) level in drinking water surpasses 50 µg/L, children under six years may experience increased levels of hyperactivity, potentially causing harm to the brain, lower intelligence quotient (IQ), and impaired attention span (Baeissa 2016). According to The World Health Organization (WHO), the highest permissible Pb(II) concentration that can be present in drinking water should not exceed 15 µg/L. In contrast, the United States Environmental Protection Agency (EPA) implements a more stringent standard of 10 µg/L (Karapinar et al. 2021; Sethy et al. 2020).

Numerous methods and strategies have been created to mitigate Pb(II) pollution in wastewater, including coagulation-flocculation, ion exchange, biosorption, solvent extraction, membrane filtration, reverse osmosis, adsorption, and photocatalysis (Siddeeg 2020). Nonetheless, these methods have drawbacks, such as generating hazardous chemical waste, inadequate metal removal, low efficiency, and substantial energy and reagent demands (Ezeonuegbu et al. 2021). Adsorption has received significant attention among these methods due to its efficiency, effectiveness, and cost-effectiveness, offering a simple and economical process with high removal efficiency, free from interfering additives (Mostafa, Yunnus & Elawwad 2022). Simultaneously, photocatalysis presents a secure, sustainable, and eco-friendly approach utilizing semiconductor materials to generate reactive species that transform harmful contaminants into harmless end products (Sagadevan et al. 2022). The combination of adsorption and photocatalysis offers the potential to enhance catalytic performance, ensuring efficient wastewater treatment by retaining pollutants close to the oxidative radicals generated during photocatalysis (Jimenez-Relinque et al. 2022). Various materials, serving as adsorbents and photocatalysts, have been harnessed to eliminate Pb(II) ions from liquid systems, including the composite material $Fe_2O_3/TiO_2$/activated carbon (Baniamerian, Teimoori & Saberi 2021), titanium dioxide, zinc oxide, and aluminum oxide (Arora 2019), magnetic nano adsorbents (Shirsath 2022), zeolite and bentonite (Thabede, Shooto & Naidoo 2020), activated carbon (Zhang et al. 2020), modified attapulgite clay (Huang et al. 2020), and $Fe_2O_3$-doped g-$C_3N_4$ nanocomposite for Pb(II) reduction (Baeissa 2016). In comparison to activated carbon, metal oxides exhibit higher Pb(II) adsorption capacities (Shi et al. 2019; Xiong et al. 2015.

Numerous metal oxides are used to remove Pb(II) ions such as MgO nanorods (Ghoniem et al. 2022), magnetic graphene oxide composites (Bao et al. 2020), $Fe_2O_3$-tea waste (Khanna et al. 2020), and CuO nanoparticles synthesized by a sputtering method (Verma et al. 2017). This method is based on adsorption, usually straightforward and efficient, but its limitation lies in the incapacity to neutralize harmful ions; instead, it merely shifts the ions from the solution to the solid adsorbent. Furthermore, when the adsorbent reaches saturation with metal ions, it transforms into solid waste, exacerbating environmental issues. For methods that use photocatalytic as well as $Bi_2O_3$-$TiO_2$ under visible light irradiation that successfully remove Pb(II) ions reached 55% (You et al. 2018) and multifunctional $TiO_2$/Alg/FeNPs beads that have efficiency removal Pb(II) ions reach 98.4% under UV light (Kanakaraju et al. 2019). Therefore, there is a need for a treatment method capable of both eliminating and detoxifying hazardous ions (Wahyuni et al. 2015). Combined adsorption and photocatalyst is a promising method to remove and also detoxify Pb(II) ions from aqueous solution.

Titanium dioxide ($TiO_2$) has garnered substantial recognition as the most prominent photocatalyst to remove Pb(II) ion due to its attractive qualities, encompassing cost-effectiveness, elevated photocatalytic efficacy, minimal toxicity, and robust chemical stability (Armaković, Savanović & Armaković 2023). However, $TiO_2$ exhibits some drawbacks, such as a significant energy band gap (Eg = 3.2 eV for anatase and Eg = 3.0 eV for rutile) and a propensity for significant annihilation of electron-hole pairs generated by light. The substantial band gap of $TiO_2$ renders it more effective in the ultraviolet light spectrum, which constitutes only approximately 5% of sunlight, in contrast to visible light (Guo et al. 2019).

One approach to enable the effective operation of $TiO_2$ in the visible light spectrum involves the

incorporation of dopants like ZnO and $SiO_2$, forming a $TiO_2$/ZnO/$SiO_2$ composite (Alshoaibi & Islam 2021). ZnO offers greater electron mobility and a prolonged lifetime for photogenerated electrons through the formation of heterojunctions, therefore $TiO_2$/ZnO/$SiO_2$ composites can effectively work in the visible light area (Zulfikar et al. 2020). Meanwhile, the addition of $SiO_2$ is intended to facilitate the formation of Ti-O-Si bonds, inhibiting the transformation of anatase into rutile, enhancing mechanical strength in $TiO_2$ thin films, and increasing the surface area of $TiO_2$ material and thereby enhancing photocatalytic activity efficiency (Wang et al. 2021). Notably, even though the composite $TiO_2$/ZnO/$SiO_2$ exhibits these favorable characteristics, its application as an adsorbent-photocatalyst for eliminating Pb(II) ions has not been reported.

In this paper, we prepared $TiO_2$/ZnO/$SiO_2$ composites via a hydrothermal method, rendering $TiO_2$ materials functional in the visible light range while maintaining a large surface area and stable anatase phase $TiO_2$, even at elevated temperatures. This study seeks to utilize the composite to employ adsorption-photocatalysis to eliminate Pb(II) ions from aqueous solutions. Our research extensively investigated how pH, contact duration, catalyst quantities, and adsorption kinetics models (pseudo-first-order and pseudo-second-order) affect the lead adsorption process. We also explored equilibrium isotherm models, including Langmuir and Freundlich. Additionally, we assessed the kinetics of photocatalysis and the percentage of removed Pb(II) ions by comparing their concentrations before and after the photocatalysis process, employing FAAS (Flame Atomic Absorption Spectrophotometry).

.

## Materials and Methods

### Materials

All materials employed in this research were of analytical grade. Tetrabuthyl ortho-titanate (TBOT) was procured from Sigma-Aldrich. Tetraethyl ortho silicate (TEOS), 2-propanol ($C_3H_8O$), nitric acid ($HNO_3$), Zinc acetate dihydrate ($Zn(CH_3COO)_2.2H_2O$), hydrochloric acid (HCl), sodium hydroxide (NaOH), and lead nitrate ($Pb(NO_3)_2$) were purchased from Merck. Additionally, demineralized water was utilized in this study.

### Synthesis of $TiO_2$/ZnO/$SiO_2$

5.56 g of TBOT was dissolved with 10 mL of 2-propanol, given Solution A. Meanwhile, solution B was produced by dissolving 3.40 g of TEOS in 10 mL of 2-propanol. Solution C was created by dissolving 4.78 g of $Zn(CH_3COO)_2$ with 1.5 mL of demineralized water and mixing it with 10 mL of 3 M NaOH. Solution A was gradually added drop by drop to 30 mL of demineralized water, adding a few drops of HCl in a 1:1 ratio until the pH reached 3, followed by the addition of Solution B. This resulted in the instant formation of white hydrous oxide precipitates. The mixture was agitated at ambient temperature for 2 h. Afterward, Solution C was added, and the stirring continued for an additional 2 h using a magnetic stirrer, resulting in a white precipitate. This precipitate was placed in a 100 mL Teflon-lined stainless steel vessel and autoclaved for 24 h at 180 °C. The precipitate material was filtered, washed with distilled water, left to dry for 12 h at ambient temperature, and then calcinized at 450 °C, yielding a white powder. The obtained $TiO_2$/ZnO/$SiO_2$ composites were characterized using XRD, UV-Vis DRS spectrophotometer, BET, and SEM-EDX. The molar composition of the three components was 30% $TiO_2$, 40% ZnO, and 30% $SiO_2$, denoted as TZS 40, reflecting the percentage of ZnO. Variations were made by keeping the $TiO_2$ component at 30% and adjusting the composition of ZnO to 10%, 20%, 30%, 40%, and 50%, with the remaining component being $SiO_2$. These variations were referred to as TZS 10, TZS 20, TZS 30, TZS 40, and TZS 50.

### Adsorption-photocatalysis for removal of Pb(II) ions

Two primary methods were utilized to remove Pb(II) ions: adsorption, involving the absorption of the Pb(II) solution into a $TiO_2$/ZnO/$SiO_2$ composite under dark conditions for 60 min, and photocatalysis, which involved removing Pb(II) ions under a mercury lamp irradiation under optimum conditions (contact time, pH, and catalyst dosage). These processes were carried out using a photocatalytic reactor with a magnetic stirrer and adjustable lamp illumination.

The pH impact was assessed by altering the pH of a 100 mg/L $Pb(NO_3)_2$ solution, adjusting it from pH 2-5 through the addition of nitric acid ($HNO_3$) and NaOH. The contact time was varied during the adsorption between 15, 30, 45, 60, 75, and 90 min to examine its influence. The catalyst dosage was tested in the range of 0.005 to 0.03 g. The adsorption studies involved dispersing 0.01 g of $TiO_2$/ZnO/$SiO_2$ powder in 50 mL of 100 mg/L $Pb(NO_3)_2$ solution at optimum pH, followed by stirring at 500 rpm for 15, 30, 45, 60, 75, and 90 min. In the isotherm

adsorption experiment, 0.01 g of $TiO_2$/ZnO/$SiO_2$ powder was dispersed under the optimum condition to adsorb 50 mL of $Pb(NO_3)_2$ solutions at concentrations of 100, 200, 400, 600, 800, and 1000 mg/L, respectively. The mixture was rotated for 60 min at 500 rpm in the darkroom. Portions of the solution were taken out following the adsorption process and then spun in a centrifuge at 6000 rpm for 15 min to separate the solid phase. The absorbance measurement in the filtered solution was conducted using a Flame Atomic Absorption Spectrometer (FAAS).

The photocatalytic process involved mixing the solution in a reactor under dark conditions for 60 min, followed by exposure to a 160-watt mercury lamp for 15, 30, 45, 60, 75, and 90 min, all conducted under optimal conditions. Following the photocatalysis process, samples from the suspension were taken and centrifuged for 15 min at 6000 rpm until separation was achieved. The samples' lead concentration was determined using a Flame Atomic Absorption Spectrometer (FAAS).

The percentage of removal of Pb(II) was calculated using the following formula:

$$\%\ Removal\ of\ Pb(II) = \frac{(C_0 - C_t)}{C_0}\ x\ 100 \qquad (1)$$

where $C_0$ and $C_t$ ($mg.L^{-1}$) refer to the initial and remaining Pb(II) concentration solution, respectively.

### CHARACTERIZATION

The X-ray diffraction (XRD) technique (utilizing Bruker D-8 Advance with Cu kα radiation, 40 kV, 40 mA) was employed to ascertain the mineral phase and size of the composite's crystallites. BET (Brunauer Emmett Teller) surface area analyzer Micromeritics Gemini VII is used for measured surface area. Scanning Electron Microscope-Energy Dispersive Spectroscopy (SEM-EDS) was conducted with a JEOL Model JSM 6360 instrument to investigate the composite's particle structure and semiquantitative analysis. The UV-Vis Diffuse Reflectance Spectrometer (DRS) was employed to ascertain the band gap energy, utilizing the Thermo Scientific Evolution 220 instrument. $BaSO_4$ (Labsphere USRS-99-010) was used as a reference standard for this purpose. The Kubelka-Munk method transformed the acquired spectra from reflectance to absorbance. The Flame Atomic Absorption Spectrometer (Agilent 200 Series AA) was utilized to measure the lead concentration.

## RESULTS AND DISCUSSION

### SYNTHESIS OF $TiO_2$/ZnO/$SiO_2$ USING HYDROTHERMAL METHOD

The $TiO_2$/ZnO/$SiO_2$ composite was adjusted to various molarity fractions at pH 3, resulting in different compositions, namely: $TiO_2$ 30%/ZnO 10%/$SiO_2$ 60% (TZS 10), $TiO_2$ 30%/ZnO 20%/$SiO_2$ 50% (TZS 20), $TiO_2$ 30%/ZnO 30%/$SiO_2$ 40% (TZS 30), $TiO_2$ 30%/ZnO 40%/$SiO_2$ 30% (TZS 40), and $TiO_2$ 30%/ZnO 50%/$SiO_2$ 20% (TZS 50). Figure 1 shows the XRD patterns for the TZS composite. The results display distinctive peaks at 2θ values of 25.31, 36.99, 37.88, 38.58, 48.03, 53.98, 55.06, 62.13, 62.74, 68.88, 70.28, 75.12, and 76.03, which are corresponding to anatase phase ($TiO_2$, PDF 00-064-0863). There are also characteristic diffraction peaks of zincite (ZnO, PDF 04-003-2106) at 2θ values of 31.77, 34.42, 36.25, 47.54, 56.59, 62.85, 66.37, 67.94, 69.08, 72.56 and 76.95. While $SiO_2$ amorphous is shown at 2θ 10° - 30°.

The Modified Scherrer formula is used to estimate the average crystallite size based on the XRD data, as illustrated herewith (Monshi, Foroughi & Monshi 2012):

$$\ln \beta = \ln \frac{K\,\lambda}{L\cos\theta} = \ln \frac{K\,\lambda}{L} + \ln \frac{1}{\cos\theta} \qquad (2)$$

where L represents the mean crystallite size; λ denotes the X-ray wavelength in nanometers; K is a constant associated with the shape of crystallites, commonly set at 0.9, θ signifies the Bragg angle in radians, and β indicates the angular FWHM (Full Width at Half Maximum) in radians.

Based on the measurement of the maximum wavelength based on the percent reflectance using UV-Vis DRS, the band gap value determines the optical characteristics of the produced $TiO_2$. Determination of the $TiO_2$ band gap is carried out indirectly using the Kubelka-Munk equation as follows (Zulfikar et al. 2020):

$$F(R\infty) = \frac{(1 - R\infty)^2}{2R\infty} \qquad (3)$$

where F(R∞) represents the Kubelka-Munk function, and R∞ is $R_{sample}/R_{standard}$.

The value of F(R∞) is proportional to the absorbance of a material, so the absorbance of a sample is carried out by plotting F(R∞) with its wavelength. Meanwhile,

the band gap measurement is determined by making a Tauc plot [F(R∞)hv] against hυ so that the equation can determine the band gap (Eg) (Enculescu et al. 2021):

$$[F(R\infty)h\nu]^2 = C_2(h\nu - E_g) \quad (4)$$

Band gap measurement, the average crystallite size, and surface area for each composite composition can be observed in Table 1. The addition of silica affects $TiO_2$ phase composition, crystallite size, surface area, and inhibits anatase-rutile polymorphic transformation when fired at high temperatures. Table 1 shows that when the TZS composite is compared to pristine $TiO_2$, the average crystallite size of the anatase phase decreases. Finer silica ones partially surround larger titania particles. The amorphous $SiO_2$ matrix serves as a barrier, impeding the interaction between titania particles, thus decelerating the coalescence of anatase and postponing the crucial point at which anatase transitions into rutile by preventing their agglomeration (Tobaldi et al. 2010; Zhou et al. 2020.

Incorporating ZnO into the $TiO_2$ catalyst may prompt recombination within the $TiO_2$ lattice structure, enhance the minimal energy required for exciting electrons, and consequently decrease the energy band gap (Mai, Tanabe & Dao 2022; Mousa et al. 2021; Rilda et al. 2019). The reduction in band gap observed in $TiO_2$/ZnO samples can be ascribed to various factors, such as the variance in functional band gaps between anatase $TiO_2$ (3.2 eV) and ZnO (3.37 eV), an augmentation in the $TiO_2$ concentration on the ZnO surface, an alignment aimed at equalizing Fermi levels across layers, and the influence of the Burstein-Moss (BM) effect. (Widyastuti et al. 2023).

Table 1 shows that the band gap will decrease when more ZnO is added to the composite. The presence of ZnO in the composite can induce charge transfer effects between $TiO_2$ and ZnO. This charge transfer can alter the electronic structure, leading to changes in the band gap, even if not too significant (Drygała et al. 2023). The metal oxides $TiO_2$ and ZnO synergize to modify their electronic states and generate charge carriers that help separate electron pairs. In a process, holes transfer from the valence band (VB) of $TiO_2$ to the valence band of ZnO, whereas electrons move from the conduction band (CB) of ZnO to that of $TiO_2$. The heterostructure simultaneously lengthens the lifespan of carriers and speeds up the semiconductor's decline in electron-hole pair recombination (Mousa et al. 2021; Xu et al. 2020). However, the more ZnO added, the less $SiO_2$ content in the composite, which reduces the composite's surface area.

SEM-EDX investigates the $TiO_2$/ZnO/$SiO_2$ composite's morphological features. Morphological particles of $TiO_2$/ZnO/$SiO_2$ synthesized using water have a uniform sphere-like shape. The EDX results for TZS 40 from Figure 2 show that the composite consists of three main elements: $TiO_2$, ZnO, and $SiO_2$.

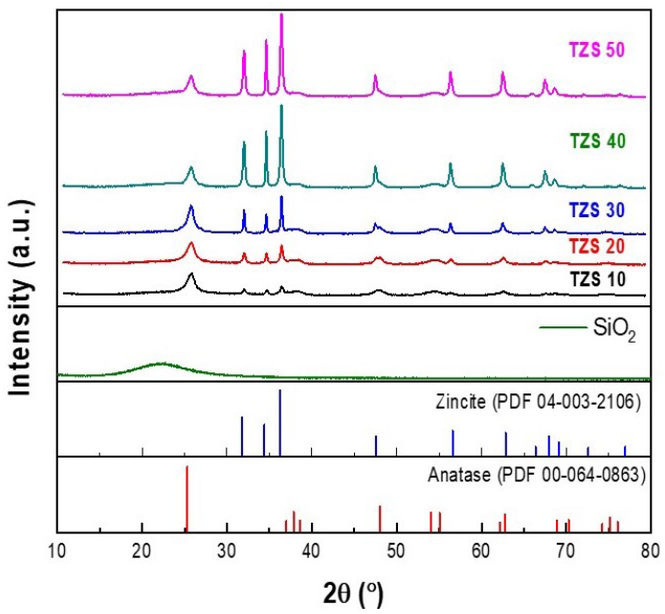


FIGURE 1. XRD pattern of $TiO_2$/ZnO/$SiO_2$ composite

TABLE 1. The average crystallite size, band gap, and surface area composite $TiO_2$/ZnO/$SiO_2$

| No | Composite composition | The average crystallite size (nm) | | Surface area (BET, $m^2/g$) | Bandgap (eV) |
|---|---|---|---|---|---|
| | | Anatase | Zincite | | |
| 1 | $TiO_2$30/ZnO10/$SiO_2$60 (TZS 10) | 13.75 | 34.01 | 195 | 3.14 |
| 2 | $TiO_2$30/ZnO20/$SiO_2$50 (TZS 20) | 15.83 | 38.53 | 156 | 3.13 |
| 3 | $TiO_2$30/ZnO30/$SiO_2$40 (TZS 30) | 19.20 | 37.58 | 129 | 3.12 |
| 4 | $TiO_2$30/ZnO40/$SiO_2$30 (TZS 40) | 16.24 | 34.66 | 120 | 3.00 |
| 5 | $TiO_2$30/ZnO50/$SiO_2$20 (TZS 50) | 14.80 | 31.99 | 114 | 3.00 |
| 6 | $TiO_2$ commercial | 22.50 | - | 42 | 3.23 |

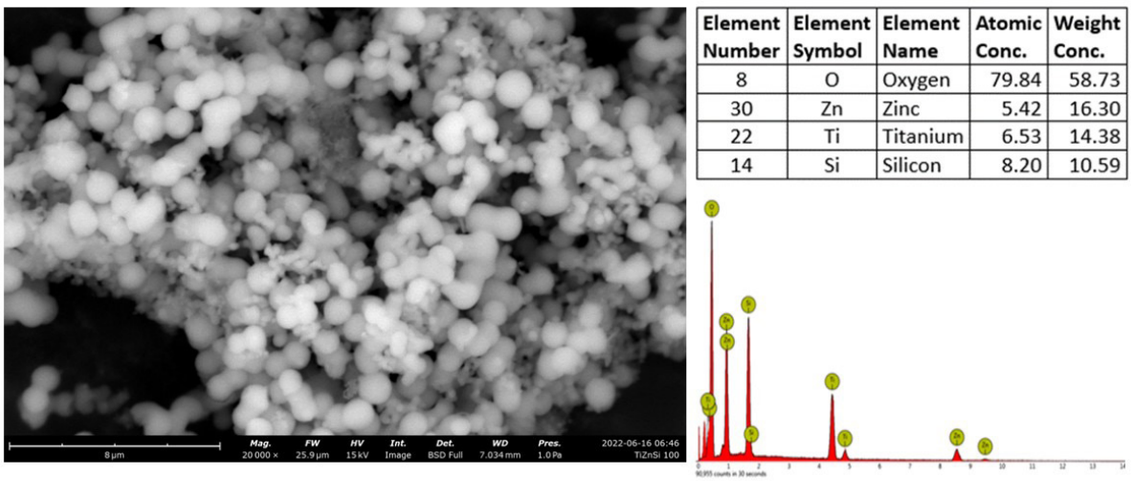


FIGURE 2. SEM-EDX image of TiO2 30%/ZnO 40%/SiO2 30% (TZS 40) composite

## ADSORPTION-PHOTOCATALYSIS FOR REMOVAL OF Pb(II) ION

*Adsorption studies*

The assessment of pH significantly influences the adsorption-photocatalytic process, directly impacting the charge distribution on the catalyst's surface (Mostafa, Yunnus & Elawwad 2022). In this experiment, the optimum pH was determined in the range of 2 to 5 by carefully adjusting the pH using NaOH and $HNO_3$. Those pH ranges were selected because, beyond a pH of 6, Pb(II) ions tend to form precipitates in the form of $Pb(OH)_2$. Subsequently, the removal of Pb(II) ions occurs not only through the adsorption-photocatalytic process but also as a result of precipitation (Nikolaychuk 2018).

The impact of several parameters in Pb(II) removal including the initial pH Pb(II) solution, amount of adsorbent, and contact time. Figure 3(a) indicates that the percentage of Pb(II) removal rises as the solution's pH rises. As the pH value increases, the adsorption of Pb(II) ions increases significantly. Competition between protons and metal ions for the adsorbent's side rises at lower pH levels. As a result, the adsorption of Pb(II) ions will decrease (Xiong et al. 2017). Declining adsorption rates could be observed at pH <3. The adsorbent surface

will interact with $H_3O^+$ at low pH levels, which prevents metal ions from accessing the surface. At pH 6, the competition between hydrogen and metal ions lessens, leading to increased lead ion adsorption on the adsorbent as pH rises (Poursani et al. 2016).

Based on the significant percentage of Pb(II) removal observed, the optimal pH was determined to be pH 4. As the pH rises, the surface charge of the adsorbent becomes more negatively charged. This causes the metal ion species ($Pb^{2+}$ and $Pb(OH)^+$) to interact heightened electrostatically with the functional groups present on the surface of the adsorbent, consequently enhancing the percentage of adsorption. Metal ions interact with the adsorbent surface through either ion exchange or the formation of hydrogen bonds (Sadr et al. 2021). This study was carried out below a pH level of 6 to investigate the impact of the optimal pH on the adsorption process, excluding the formation of $Pb(OH)_2$.

Figure 3(b) shows as more catalyst mass is added, the percentage of Pb(II) removal increases, reaching 99.88%. Increasing the catalyst mass allows more Pb(II) ions to come into contact with the catalyst surface, leading to a more significant removal percentage. However, for efficiency within the scope of this study, the optimal catalyst mass was determined to be 0.01 grams. Figure 3(c) illustrates that the longer the contact time, the higher the removal percentage. From minute 15 to minute 60, there is a notable increase in the amount of Pb(II) removed, reaching 99.83%. Beyond that, the removal percentage continues to increase but not as significantly, ultimately reaching 99.97% at the 90$^{th}$ minute. Therefore, a contact time of 60 min was identified as the ideal duration for this investigation.

Adsorption kinetics may be used to estimate the rate of Pb(II) ions removed from aqueous solution. Pseudo-first-order and pseudo-second-order kinetic models were employed to calculate the adsorption kinetics and rate constants. The equations corresponding to these models are outlined herewith (Shi et al. 2019; Zhao et al. 2010):

$$\log(q_e - q_t) = \log q_e - \frac{k_1}{2.303}\, t \tag{5}$$

$$\frac{1}{q_t} = \frac{1}{k_2 . q_e^2} + \frac{1}{q_e} \tag{6}$$

where $q_e$ and $q_t$ denote the quantity of Pb(II) adsorbed on the adsorbent surface at equilibrium and during time t ($mg.g^{-1}$); and $k_1$ stands for the rate constant for the pseudo-first-order reaction ($min^{-1}$). In contrast, t represents time (min), and $k_2$ denotes the rate constant for the pseudo-second-order reaction (g/mg.min).

Figure 4(a), 4(b), and Table 2 present the adsorption kinetic models (pseudo-first-order and pseudo-second-order) and their associated parameters. The result shows that the correlation coefficient ($R^2$) of the pseudo-second-order model concerning the adsorption outcomes surpassed the pseudo-first-order model. In addition to the $R^2$ value, the suitability of the model can be seen from the smaller the difference between the calculated $q_e$ and the experimental $q_e$ ($\Delta q_e$). From Table 2, it is observed that $\Delta q_e$ in the pseudo-second-order is smaller than that in the pseudo-first-order. This implies that the pseudo-second-order model provides the most accurate description of the adsorption process kinetics.

An adsorption isotherm is required and essential to predict the interaction of adsorbate molecules on the adsorbent surface. Relationships between solution concentrations in the solid phase and the liquid phase are called isotherms. Adsorption isotherms, which consider the maximum adsorption capacity, can determine whether a specific adsorbent is suitable for pollutant extraction (Al-Ghouti & Da'ana 2020). The Langmuir and Freundlich adsorption isotherms were modeled in this study, along with other adsorption isotherms. The following are the equations for the isotherm Langmuir and the isotherm Freundlich (Ezeonuegbu et al. 2021; Mostafa, Yunnus & Elawwad 2022):

$$\frac{1}{q_e} = \frac{1}{K_L\, q_{max}} \cdot \frac{1}{C_e} + \frac{1}{q_{max}} \tag{7}$$

$$log q_e = log K_F + \frac{1}{n} \log C_e \tag{8}$$

where $K_L$ represents the Langmuir adsorption constant ($L.g^{-1}$); $K_F$ stands for the Freundlich adsorption constant ($L.g^{-1}$); and n denotes the adsorption intensity. $C_e$ and $q_e$ are the adsorbate concentration at equilibrium ($mg.g^{-1}$) and adsorption capacity at equilibrium ($mg.g^{-1}$), respectively. The Langmuir and Freundlich adsorption isotherms were discovered by applying linear fitting to plot $C_e$ against $q_e$, as illustrated in Figure 4(b), 4(c), and Table 3.

Figure 4(d) shows that the $R^2$ value of the Freundlich isotherm is greater than that of the Langmuir isotherm, suggesting that the adsorption in this study aligns better with the Freundlich model. The Freundlich model, known for accommodating multi-layer adsorption and heterogeneity, outperforms the Langmuir isotherm in

describing the adsorption of metals by the test sorbents. This phenomenon suggests that adsorbate layers can amass on the adsorbent surface, and the energy needed for adsorption is unevenly distributed (Artioli 2008; Ezeonuegbu et al. 2021.

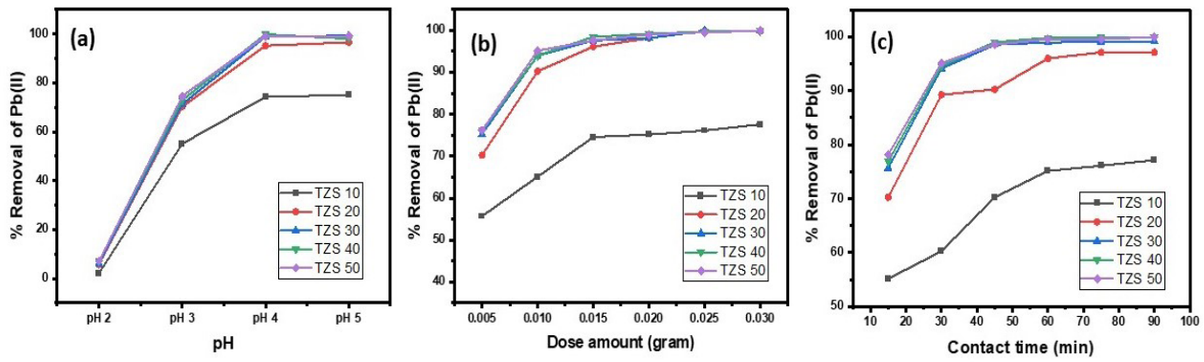


FIGURE 3. Impact of various parameters on removal Pb(II) (a) initial pH of Pb(II) solution (b) dose amount of adsorbent (c) contact time

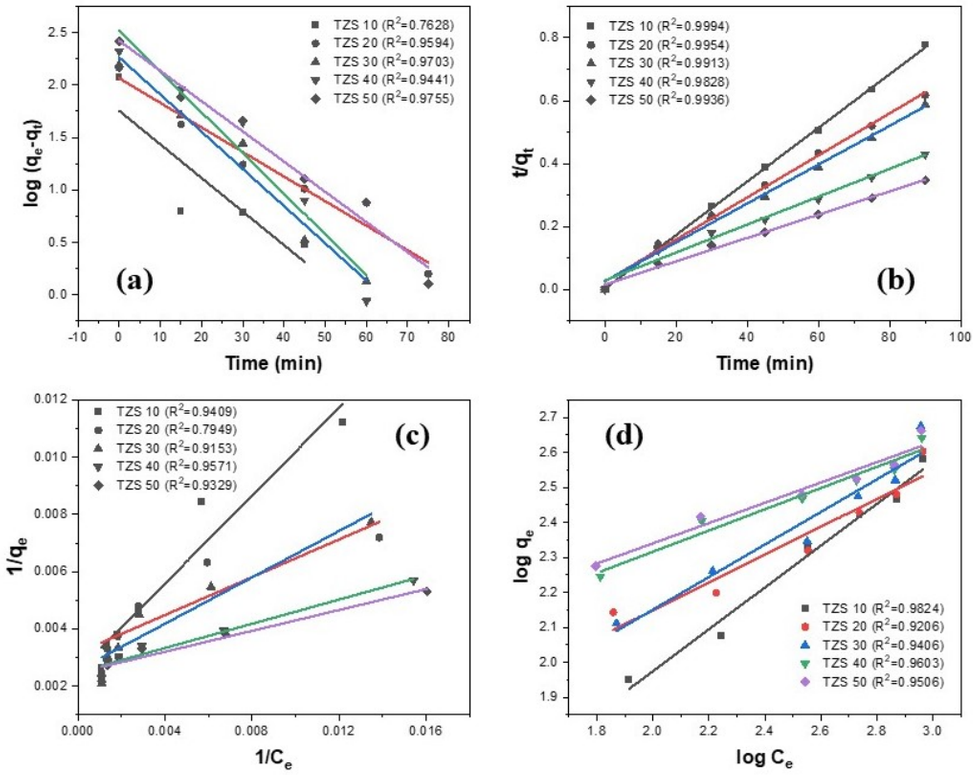


FIGURE 4. Adsorption of Pb(II) ion removal, (a) pseudo-first-order kinetic, (b) pseudo-second-order kinetic, (c) Langmuir isotherm, (d) Freundlich isotherm

TABLE 2. Kinetic parameters for adsorption of Pb(II) ion using pseudo-first-order and pseudo-second-order

| Catalyst | Kinetic model | | | | | | |
|---|---|---|---|---|---|---|---|
| | Pseudo-first-order | | | Pseudo-second-order | | | |
| | $k_1$ ($min^{-1}$) | $q_e$ ($mg.g^{-1}$) | $R^2$ | $k_2$ (g/mg.min) | $q_e$ ($mg.g^{-1}$) | $R^2$ | $q_e$ exp (mg/g) |
| TZS 10 | 0.0737 | 56.84 | 0.7628 | 0.0226 | 117.65 | 0.9994 | 119.05 |
| TZS 20 | 0.0539 | 115.82 | 0.9594 | 0.0017 | 149.25 | 0.9954 | 145.71 |
| TZS 30 | 0.0815 | 183.57 | 0.9703 | 0.0014 | 161.29 | 0.9913 | 155.79 |
| TZS 40 | 0.0894 | 321.49 | 0.9441 | 0.0007 | 227.27 | 0.9828 | 210.08 |
| TZS 50 | 0.0663 | 264.24 | 0.9663 | 0.0008 | 270.27 | 0.9936 | 259.68 |

TABLE 3. Isotherm parameters of Pb(II) ion removal

| Catalyst | Adsorption isotherms | | | | | |
|---|---|---|---|---|---|---|
| | Langmuir | | | Freundlich | | |
| | $q_{max}$ (mg/g) | $K_L$ ($L.mg^{-1}$) | $R^2$ | $K_F$ (mg/g $(mg/L)^{-1/n}$) | n | $R^2$ |
| TZS 10 | 400.00 | 0.0033 | 0.9409 | 6.0214 | 1.6734 | 0.9824 |
| TZS 20 | 312.50 | 0.0097 | 0.7949 | 22.6048 | 2.5164 | 0.9206 |
| TZS 30 | 384.62 | 0.0064 | 0.9153 | 16.5806 | 2.1482 | 0.9406 |
| TZS 40 | 400.00 | 0.0118 | 0.9571 | 51.2153 | 3.2971 | 0.9603 |
| TZS 50 | 400.00 | 0.0137 | 0.9526 | 57.6634 | 3.4531 | 0.9506 |

*Photocatalytic studies*

Pb(II) metal ions were removed using adsorption by stirring for 60 min in a reactor at dark conditions. The photocatalytic reaction was then carried out by irradiation with a 160-watt mercury lamp with variations in irradiation time for 15, 30, 45, 60, 75, and 90 min. In photocatalysis, the adsorption of organic contaminants on the photocatalyst's surface is crucial for heterogeneous photocatalytic reactions.

Figure 5(a) shows the relationship between photocatalysis and adsorption, demonstrating that the addition of Zn composition (TZS 10-TZS 50) results in Pb(II) removal rates of 23.81-50.41% during the adsorption phase. Subsequently, Pb(II) removal increases to 87.78-99.58% during the photocatalytic process. Remarkably, the TZS 40 composition exhibits the most effective synergistic effect, when compared to other composites. For the adsorption process using TZS 40 composite, the removal of Pb(II) reached 41.84%, with a pseudo-first-order rate constant ($k_1$) of 0.0553 $min^{-1}$ and a coefficient correlation of 0.9722, followed by the photocatalytic process achieving the highest Pb(II) elimination percentage (99.58%) in optimum conditions. The effect of ZnO addition on $TiO_2$/ZnO/$SiO_2$ composite also greatly influences the Pb(II) removal percentage. The more ZnO composition added, the higher the percentage of removal. However, the increase in Pb(II) removal percentage is not so significant when ZnO addition is above 30% mole fraction. The intensity of the XRD pattern and the bandgap value between TZS 40 and

50 were not significantly different. Therefore, TZS 40 is suggested as the most favourable composite for removal of Pb(II) in this study.

An essential consideration when optimizing conditions for photocatalysis activity is photocatalysis kinetics, which can provide valuable insights into the reaction rate constant, significantly influencing the overall reaction rate (Song et al. 2021). The pseudo-first-order and pseudo-second-order reaction kinetics model technique is used to study the kinetics of photocatalysis. In the pseudo-first-order model, an adsorbate ion is absorbed by a single active site on the adsorbent surface. Conversely, the pseudo-second-order model suggests that an adsorbate ion can be adsorbed onto two active sites present on the adsorbent surface (Mustapha et al. 2019). The equations of pseudo-first-order and pseudo-second-order are as follows (Kaur, Kumari & Sharma 2020):

$$ln[(C_t] = -k_1 t + ln[C_0] \quad (9)$$

$$\frac{1}{[C_t]} = k_2 t + \frac{1}{[C_0]} \quad (10)$$

where $C_0$ represents the initial concentration of the Pb(II) solution; and $C_t$ represents the concentration of Pb(II) subsequent to radiation at a specific time ($mg.L^{-1}$). The variable t signifies the duration of irradiation in minutes, $k_1$ denotes the rate constant for the pseudo-first-order reaction ($min^{-1}$), and $k_2$ signifies the rate constant for the pseudo-second-order reaction ($mg^{-1}Lmin^{-1}$). Figure 6 and Table 4 compare reaction rate and correlation coefficient values based on pseudo-first-order and pseudo-second-order. Judging from the value of the correlation coefficient ($R^2$), the Pb(II) ion removal reaction follows a pseudo-first-order model with an $R^2$ value (0.9669-0.9902) that is close to the value of one.

The removal of Pb(II) ions from a simulated $Pb(NO_3)_2$ solution was then performed using each composite under optimum conditions (pH, dose amount, and contact time). The efficiency of removal results was compared with pure $TiO_2$, ZnO, and $SiO_2$ photocatalysts. Figure 5(b) compares Pb(II) removal in an aqueous solution using $TiO_2$/ZnO/$SiO_2$ composite with pure $TiO_2$, pure ZnO, and pure $SiO_2$. $TiO_2$/ZnO/$SiO_2$ composite can reach 99.58% removal of Pb(II), while compared with pure $TiO_2$, pure ZnO, and pure $SiO_2$, the Pb(II) removal results reached 6.38%, 11.07%, and 8.07%, respectively. When $TiO_2$ particles are dispersed within a porous $SiO_2$ matrix, they are surrounded by a high surface area, which increases the overall surface area of the composite (Hikmah et al. 2022). Therefore, the surface area of TZS will be larger than commercial $TiO_2$. As the surface area increases, the adsorption process will be more effective. Likewise in the process of photocatalysis, both $TiO_2$ and ZnO are similar semiconductors with wide band gaps (3.2 eV for $TiO_2$ anatase and 3.4 eV for ZnO). Therefore, both ZnO and $TiO_2$ photocatalysts have been limited range of light response to UV region. The formation of $TiO_2$/ZnO nanocomposites has been proposed for the design of photocatalytic systems to decrease the rate of recombination regarding individual semiconductors, thus lowering the bandgap (from 3.2 eV to 3.0 eV). This bandgap reduction to 3.0 eV is equivalent to 400 nm which corresponds to the absorption in the mercury lamp being used (Fonseca-Cervantes et al. 2020). Therefore, TZS performs better than its individual materials.

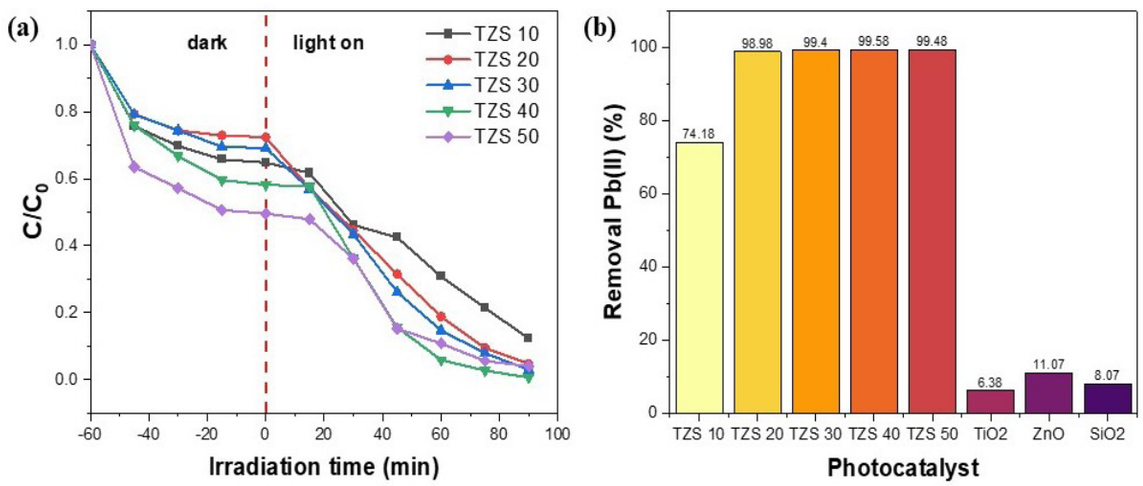


FIGURE 5. (a) Adsorption-photocatalytic removal of Pb(II), (b) Photocatalytic removal of Pb(II) ions using $TiO_2$/ZnO/$SiO_2$ composites with various compositions

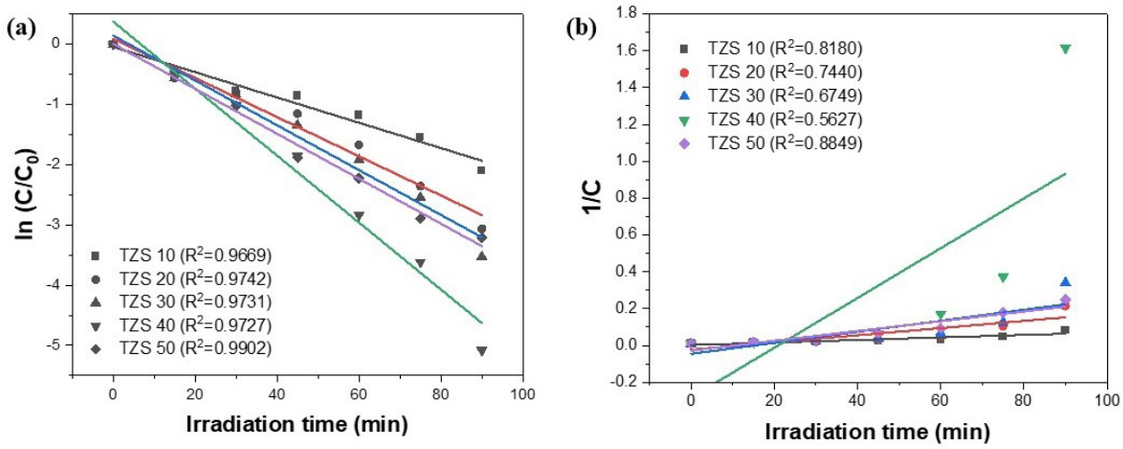


FIGURE 6. Photocatalytic kinetics of removal Pb(II) ion, (a) pseudo-first-order (b) pseudo-second-order

TABLE 4. Photocatalytic kinetic parameters of Pb(II) ion removal

| Catalyst | Kinetic models | | | |
|---|---|---|---|---|
| | Pseudo-first-order | | Pseudo-second-order | |
| | $K_1$ ($min^{-1}$) | $R^2$ | $K_2$ ($mg^{-1}Lmin^{-1}$) | $R^2$ |
| TZS 10 | 0.0210 | 0.9669 | 0.0007 | 0.8180 |
| TZS 20 | 0.0325 | 0.9742 | 0.0020 | 0.7439 |
| TZS 30 | 0.0372 | 0.9731 | 0.0030 | 0.6749 |
| TZS 40 | 0.0553 | 0.9722 | 0.0135 | 0.5624 |
| TZS 50 | 0.0361 | 0.9884 | 0.0026 | 0.8822 |

## PROPOSED MECHANISM FOR THE REMOVAL OF Pb(II) IONS

This adsorption-photocatalytic work is carried out in the pH range 2-5, thus, the Pb species formed in the Pb-$H_2O$ system are $Pb^{2+}$ and $Pb(OH)^+$ (Nikolaychuk 2018) and the thermodynamic activity - pH diagram of Pb(II).. Initially, lead ions species from the solution are adsorbed onto the surface of TZS nanoparticles. The adsorption process involves three key phases: film diffusion, surface adsorption, and intraparticle diffusion. When the initial solution pH rises, more metal ions are exchanged with the negatively charged adsorbent surface, increasing the adsorption percentage (Yang et al. 2020). This adsorption can occur through ion exchange mechanisms as shown in Figure 7(a) and the following reaction (Mostafa, Yunnus, and Elawwad 2022):

$$2(\text{-ROH}) + Pb^{2+} \longrightarrow 2(\text{RO})Pb + 2H^+$$

$$\text{-ROH} + Pb(OH)+ \longrightarrow (\text{-RO})Pb(OH) + H^+$$

where R represents the adsorbent sites.

Figure 7(a) illustrates the process of metal ion adsorption on the adsorbent surface through ion exchange, which leads to the release of $H^+$ ions into the solution, thereby facilitating the exchange of $Pb^{2+}$ ions and eventually leading to the formation of PbO compounds. In the photocatalytic process, heterogeneous photocatalysis using $TiO_2$ as a semiconductor and UV/visible light is a newly developed method capable of oxidizing or reducing various contaminants (Murruni et al. 2008). Pb(II) is deposited on the catalyst surface as a free ion or complex. Pb(II) can participate in oxidative and reductive photocatalytic reactions. However, the lead was just adsorbed on the catalyst surface rather than perhaps being reduced (Kabra, Chaudhary & Sawhney 2008). Pb(II) ion removal can occur by either oxidative or reductive mechanisms. However, a reductive mechanism is a limited route because it is unfavorable due to thermodynamic constraints to reduce Pb(I) directly by conduction band electrons. To further confirm what phase of Pb is formed after adsorption-photocatalytic treatment, the adsorbent ($TiO_2$/ZnO/$SiO_2$ composite) and adsorbate (Pb(II) ions) were then analyzed using XRD.

Figure 7(b) shows that the phases formed on the adsorbent and adsorbate are anatase, zincite, and litharge. Anatase and zincite are the phases on the adsorbent/photocatalyst, while the adsorbate is litharge. Litharge (PDF 01-085-1414) is a lead mono oxide (PbO), yellowish solid that is adsorbed in $TiO_2$/ZnO/$SiO_2$ composite. In this phenomenon, metal ions are oxidized by positive holes produced by $TiO_2$ during illumination. On the other hand, electrons produced by the conduction band may oxidize oxygen or protons dissolved in water to create superoxide ions ($O_2^-$). PbO is the main product of the $Pb^{2+}$ reaction with $O_2^-$ radical (Tanaka, Harada & Murata 1986).

$$2O_2 + 2e^- \longrightarrow 2O_2^-$$

$$2Pb^{2+} + 4O_2^- \longrightarrow 2PbO + 3O_2$$

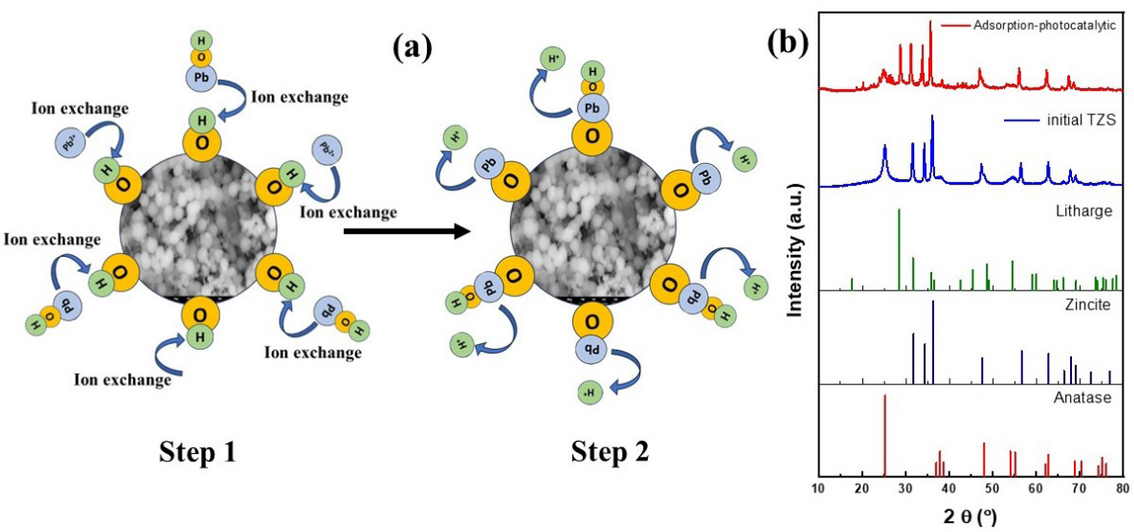


FIGURE 7. Illustration of Pb(II) ions adsorption process on the adsorbent surface via (a) ion exchange mechanism and (b) XRD analysis results of the Pb phase through adsorption-photocatalytic

## CONCLUSION

$TiO_2$/ZnO/$SiO_2$ nanocomposite synthesized using a hydrothermal technique at 180 °C for 24 h was extensively explored in this study to remove Pb(II) via an adsorption-photocatalytic process. The impact of pH, the amount of adsorbent-photocatalyst employed, and contact time were examined on the adsorption-photocatalytic process and removal effectiveness. Through various batch experiments, the optimum conditions of these parameters were discovered. The best results were

achieved with a pH of 4, $Pb(NO_3)_2$ initial concentration of 100 mg/L within a volume of 50 mL, the addition of 0.01 grams of the composite, and an irradiation duration of 60 min. Adsorption equilibration was conducted in the dark for 60 min, followed by irradiation with a 160-watt mercury lamp. The kinetic adsorption of Pb(II) removal follows the pseudo-second-order, while the adsorption isotherm follows the Freundlich isotherm. Meanwhile, for the kinetics of photocatalysis, the removal of Pb(II) ions follows pseudo-first-order, with the percentage of Pb(II) removal reaching 99.58%. After the adsorption-photocatalytic, a yellowish precipitate was formed and analyzed using XRD. The results of XRD analysis of a yellowish precipitate show that the Pb phase formed is PbO. The adsorbent-photocatalyst $TiO_2$/ZnO/$SiO_2$ nanocomposite is an effective, efficient, and promising method to eliminate Pb(II) contamination from the environment.

## ACKNOWLEDGMENTS

The authors express their gratitude to the Ministry of Education, Culture, Research, and Technology of the Republic of Indonesia for providing financial support for this research. The authors also thank Institut Teknologi Bandung and the Indonesian Center for Ceramics for facilitating this research.

## REFERENCES

Al-Ghouti, M.A. & Da'ana, D.A. 2020. Guidelines for the use and interpretation of adsorption isotherm models: A review. *Journal of Hazardous Materials* 393: 122383. https://doi.org/10.1016/j.jhazmat.2020.122383

Alshoaibi, A. & Islam, S. 2021. Thermally stable ZnO doped $SiO_2$–$TiO_2$ nanocomposite based opto-chemical sensor. *Materials Chemistry and Physics* 267: 124687. https://doi.org/10.1016/j.matchemphys.2021.124687

Armaković, S.J., Savanović, M.M. & Armaković, S. 2023. Titanium dioxide as the most used photocatalyst for water purification: An overview. *Catalysts* 13(1): 26. https://doi.org/10.3390/catal13010026

Arora, R. 2019. Adsorption of heavy metals-A review. *Materials Today: Proceedings* 18(7): 4745-4750. https://doi.org/10.1016/j.matpr.2019.07.462

Artioli, Y. 2008. The chemistry of adsorption. *Encyclopedia of Ecology* 5: 60-65. https://www.sciencedirect.com/science/article/pii/B9780080454054002524

Baeissa, E.S. 2016. Photocatalytic removal of Pb ions from aqueous solution using $Fe_2O_3$ doped in G-$C_3N_4$ nanocomposite under visible light. *Frontiers in Nanoscience and Nanotechnology* 2(2): 100-106. https://doi.org/10.15761/fnn.1000116

Balali-Mood, M., Naseri, K., Tahergorabi, Z., Khazdair, M.R. & Sadeghi, M. 2021. Toxic mechanisms of five heavy metals: Mercury, lead, chromium, cadmium, and arsenic. *Frontiers in Pharmacology* 12: 643972. https://doi.org/10.3389/fphar.2021.643972

Baniamerian, H., Teimoori, M. & Saberi, M. 2021. $Fe_2O_3$/$TiO_2$/activated carbon nanocomposite with synergistic effect of adsorption and photocatalysis. *Chemical Engineering and Technology* 44(1): 130-139. https://doi.org/10.1002/ceat.202000403

Bao, S., Yang, W., Wang, Y., Yu, Y. & Sun, Y. 2020. One-pot synthesis of magnetic graphene oxide composites as an efficient and recoverable adsorbent for Cd(II) and Pb(II) removal from aqueous solution. *Journal of Hazardous Materials* 381: 120914. https://doi.org/10.1016/j.jhazmat.2019.120914

Drygała, A., Starowicz, Z., Gawlińska-Nęcek, K., Karolus, M., Lipiński, M., Jarka, P., Matysiak, W., Tillová, E., Palček, P. & Tański, T. 2023. Hybrid mesoporous $TiO_2$/ZnO electron transport layer for efficient perovskite solar cell. *Molecules* 28(15): 5656. https://doi.org/10.3390/molecules28155656

Enculescu, M., Costas, A., Evanghelidis, A. & Enculescu, I. 2021. Fabrication of ZnO and $TiO_2$ nanotubes via flexible electro-spun nanofibers for photocatalytic applications. *Nanomaterials* 11(5): 1305. https://doi.org/10.3390/nano11051305

Ezeonuegbu, B.A., Machido, D.A., Whong, C.M.Z., Japhet, W.S., Alexiou, A., Elazab, S.T., Qusty, N., Yaro, C.A. & Batiha, G.E.S. 2021. Agricultural waste of sugarcane bagasse as efficient adsorbent for lead and nickel removal from untreated wastewater: Biosorption, equilibrium isotherms, kinetics and desorption studies. *Biotechnology Reports* 30: e00614. https://doi.org/10.1016/j.btre.2021.e00614

Fonseca-Cervantes, O.R., Pérez-Larios, A., Arellano, V.H.R., Sulbaran-Rangel, B. & González, C.A.G. 2020. Effects in band gap for photocatalysis in $TiO_2$ support by adding gold and ruthenium. *Processes* 8(9): 1032. https://doi.org/10.3390/pr8091032

Ghoniem, M.G., Ben Aissa, M.A., Ali, F.A.M. & Khairy, M. 2022. Efficient and rapid removal of Pb(II) and Cu(II) heavy metals from aqueous solutions by MgO nanorods. *Inorganics* 10(12): 256. https://doi.org/10.3390/inorganics10120256

Guo, Q., Zhou, C., Ma, Z. & Yang, X. 2019. Fundamentals of $TiO_2$ photocatalysis: Concepts, mechanisms, and challenges. *Advanced Materials* 31(50): 1901997. https://doi.org/10.1002/adma.201901997

Hikmah, N., Agustiningsih, D., Nuryono & Kunarti, E.S. 2022. Preparation of iron-doped $SiO_2$/$TiO_2$ using silica from sugarcane bagasse ash for visible light degradation of congo red. *Indonesian Journal of Chemistry* 22(2): 402-412. https://doi.org/10.22146/ijc.69501

Huang, R., Lin, Q., Zhong, Q., Zhang, X., Wen, X. & Luo, H. 2020. Removal of Cd(II) and Pb(II) from aqueous solution by modified attapulgite clay. *Arabian Journal of Chemistry* 13(4): 4994-5008. https://doi.org/10.1016/j.arabjc.2020.01.022

Jimenez-Relinque, E., Lee, S.F., Plaza, L. & Castellote, M. 2022. Synergetic adsorption–Photocatalysis process for water treatment using $TiO_2$ supported on waste stainless steel slag. *Environmental Science and Pollution Research* 29(26): 39712-39722. https://doi.org/10.1007/s11356-022-18728-8

Kabra, K., Chaudhary, R. & Sawhney, R.L. 2008. Solar photocatalytic removal of Cu(II), Ni(II), Zn(II) and Pb(II): Speciation modeling of metal-citric acid complexes. *Journal of Hazardous Materials* 155(3): 424-432. https://doi.org/10.1016/j.jhazmat.2007.11.083

Kanakaraju, D., Mohamad Shahdad, N.R., Lim, Y.C. & Pace, A. 2019. Concurrent removal of Cr(III), Cu(II), and Pb(II) ions from water by multifunctional $TiO_2$/Alg/FeNPs beads. *Sustainable Chemistry and Pharmacy* 14: 100176. https://doi.org/10.1016/j.scp.2019.100176

Karapinar, H.S., Kilicel, F., Ozel, F. & Sarilmaz, A. 2021. Fast and effective removal of Pb(II), Cu(II) and Ni(II) ions from aqueous solutions with $TiO_2$ nanofibers: Synthesis, adsorption-desorption process and kinetic studies. *International Journal of Environmental Analytical Chemistry* 103(16): 4731-4751. https://doi.org/10.1080/03067319.2021.1931162

Kaur, M., Kumari, S. & Sharma, P. 2020. Removal of Pb (II) from aqueous solution using nanoadsorbent of *Oryza sativa* husk: Isotherm, kinetic and thermodynamic studies. *Biotechnology Reports* 25: e00410. https://doi.org/10.1016/j.btre.2019.e00410

Khanna, M., Mathur, A., Dubey, A.K., McLaughlin, J., Moirangthem, I., Wadhwa, S., Singh, D. & Kumar, R. 2020. Rapid removal of lead(II) ions from water using iron oxide-tea waste nanocomposite - A kinetic study. *IET Nanobiotechnology* 14(4): 275-280. https://doi.org/10.1049/iet-nbt.2019.0312

Mai, H.P., Tanabe, S. & Dao, M.T. 2022. The effect of ZnO addition into $TiO_2$ nano photocatalyst on the degradation of dye compound in aqueous solution under UV-LED irradiation. *Research Square* https://doi.org/10.21203/rs.3.rs-1784067/v1

Monshi, A., Foroughi, M.R. & Monshi, M.R. 2012. Modified Scherrer equation to estimate more accurately nano-crystallite size using XRD. *World Journal of Nano Science and Engineering* 2(3): 154-160. https://doi.org/10.4236/wjnse.2012.23020

Mostafa, N.G., Yunnus, A.F. & Elawwad, A. 2022. Adsorption of Pb(II) from water onto ZnO, $TiO_2$, and $Al_2O_3$: Process study, adsorption behaviour, and thermodynamics. *Adsorption Science and Technology* 2022: 7582756. https://doi.org/10.1155/2022/7582756

Mousa, H.M., Alenezi, J.F., Mohamed, I.M.A., Yasin, A.S., Hashem, A.F.M. & Abdal-Hay, A. 2021. Synthesis of $TiO_2$@ZnO heterojunction for dye photodegradation and wastewater treatment. *Journal of Alloys and Compounds* 886: 161169. https://doi.org/10.1016/j.jallcom.2021.161169

Murruni, L., Conde, F., Leyva, G. & Litter, M.I. 2008. Photocatalytic reduction of Pb(II) over $TiO_2$: New insights on the effect of different electron donors. *Applied Catalysis B: Environmental* 84(3-4): 563-569. https://doi.org/10.1016/j.apcatb.2008.05.012

Mustapha, S., Shuaib, D.T., Ndamitso, M.M., Etsuyankpa, M.B., Sumaila, A., Mohammed, U.M. & Nasirudeen, M.B. 2019. Adsorption isotherm, kinetic and thermodynamic studies for the removal of Pb(II), Cd(II), Zn(II) and Cu(II) ions from aqueous solutions using *Albizia lebbeck* pods. *Applied Water Science* 9: 142. https://doi.org/10.1007/s13201-019-1021-x

Nikolaychuk, P.A. 2018. The revised potential – pH diagram for Pb – $H_2O$ system. *Ovidius University Annals of Chemistry* 29(2): 55-67. https://doi.org/10.2478/auoc-2018-0008

Poursani, A.S., Nilchi, A., Hassani, A., Shariat, S.M. & Nouri, J. 2016. The synthesis of nano $TiO_2$; and its use for removal of lead ions from aqueous solution. *Journal of Water Resource and Protection* 8(4): 438-448. https://doi.org/10.4236/jwarp.2016.84037

Rilda, Y., Damara, D., Syukri, Putri, Y.E., Refinel & Agustien, A. 2019. Synthesis of ZnO-$TiO_2$/chitosan nanorods by using precipitation methods and studying their structures and optics properties at different precursor molar compositions. *IOP Conference Series: Earth and Environmental Science* 217: 012015. https://doi.org/10.1088/1755-1315/217/1/012015

Sadr, S., Langroudi, A.E., Nejaei, A., Rabiee, A. & Mansouri, N. 2021. Arsenic and lead removal from water by nano-photocatalytic systems (a review). *Anthropogenic Pollution Journal* 5(1): 72-80. https://doi.org/10.22034/ap.2021.1924078.1094

Sagadevan, S., Fatimah, I., Egbosiub, T.C., Alshahateet, S.F., Anita Lett, J., Weldegebrieal, G.K., Le, M.V. & Johan, M.R. 2022. Photocatalytic efficiency of titanium dioxide for dyes and heavy metals removal from wastewater. *Bulletin of Chemical Reaction Engineering & Catalysis* 17(2): 430-450. https://doi.org/10.9767/BCREC.17.2.13948.430-450

Sethy, N.K., Arif, Z., Mishra, P.K. & Kumar, P. 2020. Green synthesis of $TiO_2$ nanoparticles from *Syzygium cumini* extract for photo-catalytic removal of lead (Pb) in explosive industrial wastewater. *Green Processing and Synthesis* 9(1): 171-181. https://doi.org/10.1515/gps-2020-0018

Shi, Q., Terracciano, A., Zhao, Y., Wei, C., Christodoulatos, C. & Meng, X. 2019. Evaluation of metal oxides and activated carbon for lead removal: Kinetics, isotherms, column tests, and the role of co-existing ions. *Science of the Total Environment* 648: 176-183. https://doi.org/10.1016/j.scitotenv.2018.08.013

Shirsath, D.S. 2022. Synthesis and application of magnetic nanoadsorbent in removal of toxic metals from aqueous solution. *Journal of Water and Environmental Nanotechnology* 7(1): 89-100. https://doi.org/10.22090/jwent.2022.01.007

Siddeeg, S.M. 2020. A novel synthesis of $TiO_2$/GO nanocomposite for the uptake of $Pb^{2+}$ and $Cd^{2+}$ from wastewater. *Materials Research Express* 7(2): 025038. https://doi.org/10.1088/2053-1591/ab7407

Song, W., Zhao, J., Xie, X., Liu, W., Liu, S., Chang, H. & Wang, C. 2021. Novel BiOBr by compositing low-cost biochar for efficient ciprofloxacin removal: The synergy of adsorption and photocatalysis on the degradation kinetics and mechanism insight. *RSC Advances* 11(25): 15369-15379. https://doi.org/10.1039/d1ra00941a

Tanaka, K., Harada, K. & Murata, S. 1986. Photocatalytic deposition of metal ions onto $TiO_2$ powder. *Solar Energy* 36(2): 159-161. https://doi.org/10.1016/0038-092X(86)90121-0

Thabede, P.M., Shooto, N.D. & Naidoo, E.B. 2020. Removal of methylene blue dye and lead ions from aqueous solution using activated carbon from black cumin seeds. *South African Journal of Chemical Engineering* 33: 39-50. https://doi.org/10.1016/j.sajce.2020.04.002

Tobaldi, D.M., Tucci, A., Škapin, A.S. & Esposito, L. 2010. Effects of $SiO_2$ addition on $TiO_2$ crystal structure and photocatalytic activity. *Journal of the European Ceramic Society* 30(12): 2481-2490. https://doi.org/10.1016/j.jeurceramsoc.2010.05.014

Verma, M., Tyagi, I., Chandra, R. & Gupta, V.K. 2017. Adsorptive removal of Pb (II) ions from aqueous solution using CuO nanoparticles synthesized by sputtering method. *Journal of Molecular Liquids* 225: 936-944. https://doi.org/10.1016/j.molliq.2016.04.045

Wahyuni, E.T., Mochammad, R.S., Mahira, N.S., Lestari, N.D., Syoufian, A. & Abdillah Nasir, T. 2022. Enhancement of $TiO_2$ activity under visible light by doping S element from sulfur core for Pb(II) photo-oxidation. *Reaction Kinetics, Mechanisms and Catalysis* 135(5): 2783-2796. https://doi.org/10.1007/s11144-022-02268-w

Wahyuni, E., Aprilita, N., Hatimah, H., Wulandari, A. & Mudasir, M. 2015. Removal of toxic metal ions in water by photocatalytic method. *American Chemical Science Journal* 5(2): 194-201. https://doi.org/10.9734/acsj/2015/13807

Wang, X., Ding, H., Sun, S., Zhang, H., Zhou, R., Li, Y., Liang, Y. & Wang, J. 2021. Preparation of a temperature-sensitive superhydrophobic self-cleaning $SiO_2$-$TiO_2$@PDMS coating with photocatalytic activity. *Surface and Coatings Technology* 408: 126853. https://doi.org/10.1016/j.surfcoat.2021.126853

Widyastuti, E., Chiu, C.T., Hsu, J.L. & Lee, Y.C. 2023. Photocatalytic antimicrobial and photostability studies of $TiO_2$/ZnO thin films. *Arabian Journal of Chemistry* 16(8): 105010. https://doi.org/10.1016/j.arabjc.2023.105010

Xiong, C., Wang, W., Tan, F., Luo, F., Chen, J. & Qiao, X. 2015. Investigation on the efficiency and mechanism of Cd(II) and Pb(II) removal from aqueous solutions using MgO nanoparticles. *Journal of Hazardous Materials* 299: 664-674. https://doi.org/10.1016/j.jhazmat.2015.08.008

Xiong, Z., Lei, Z., Ma, S., Chen, X., Gong, B., Zhao, Y., Zhang, J., Zheng, C. & Wu, J.C.S. 2017. Photocatalytic $CO_2$ reduction over V and W codoped $TiO_2$ catalyst in an internal-illuminated honeycomb photoreactor under simulated sunlight irradiation. *Applied Catalysis B: Environmental* 219: 412-424. https://doi.org/10.1016/j.apcatb.2017.07.078

Xu, K., Liu, Z., Qi, S., Yin, Z., Deng, S., Zhang, M. & Sun, Z. 2020. Construction of Ag-modified $TiO_2$/ZnO heterojunction nanotree arrays with superior photocatalytic and photoelectrochemical properties. *RSC Advances* 10(57): 34702-34711. https://doi.org/10.1039/d0ra06596j

Yang, X., Guo, N., Yu, Y., Li, H., Xia, H. & Yu, H. 2020. Synthesis of magnetic graphene oxide-titanate composites for efficient removal of Pb(II) from wastewater: Performance and mechanism. *Journal of Environmental Management* 256: 109943. https://doi.org/10.1016/j.jenvman.2019.109943

Yang, Z.P. & Zhang, C.J. 2010. Kinetics of photocatalytic reduction of Pb(II) on nanocrystalline $TiO_2$ coatings: A quartz crystal microbalance study. *Thin Solid Films* 518(21): 6006-6009. https://doi.org/10.1016/j.tsf.2010.06.041

You, S., Hu, Y., Liu, X. & Wei, C. 2018. Synergetic removal of Pb(II) and dibutyl phthalate mixed pollutants on $Bi_2O_3$-$TiO_2$ composite photocatalyst under visible light. *Applied Catalysis B: Environmental* 232: 288-298. https://doi.org/10.1016/j.apcatb.2018.03.025

Zhang, Y., Song, X., Zhang, P., Gao, H., Ou, C. & Kong, X. 2020. Production of activated carbons from four wastes via one-step activation and their applications in $Pb^{2+}$ adsorption: Insight of ash content. *Chemosphere* 245: 125587. https://doi.org/10.1016/j.chemosphere.2019.125587

Zhao, X., Jia, Q., Song, N., Zhou, W. & Li, Y. 2010. Adsorption of Pb(II) from an aqueous solution by titanium dioxide/carbon nanotube nanocomposites: Kinetics, thermodynamics, and isotherms. *Journal of Chemical and Engineering Data* 55(10): 4428-4433. https://doi.org/10.1021/je100586r

Zhou, K., Ding, Y., Zhang, L., Wu, H. & Guo, J. 2020. Synthesis of mesoporous ZnO/$TiO_2$-$SiO_2$ composite material and its application in photocatalytic adsorption desulfurization without the addition of an extra oxidant. *Dalton Transactions* 49(5): 1600-1612. https://doi.org/10.1039/c9dt04454j

Zulfikar, M.A., Chandra, A.D., Rusnadi, Setiyanto, H., Handayani, N. & Wahyuningrum, D. 2020. $TiO_2$/ZnO nanocomposite photocatalyst: Synthesis, characterization and their application for degradation of humic acid from aqueous solution. *Songklanakarin Journal of Science and Technology* 42(2): 439-446. https://doi.org/10.14456/sjst-psu.2020.57

*Corresponding author: email: zulfikar@chem.itb.ac.id